

## Photoelectron angular distribution measurements of $s$ and $d$ electrons from the photodetachment of $V^-$ at visible wavelengths

D. Calabrese

*Department of Physics, Sierra College, Rocklin, California 95677, USA*

A. M. Covington, W. W. Williams,\* D. L. Carpenter,† and J. S. Thompson

*Department of Physics and Chemical Physics Program, University of Nevada, Reno, Nevada 89557-0058, USA*

T. J. Kvale

*Department of Physics and Astronomy, The University of Toledo, Toledo, Ohio 43606-3390, USA*

(Received 16 July 2004; published 22 April 2005)

Photodetached  $d$ -electron angular distributions have been measured for the processes  $V^-(3d^44s^2)^5D+h\nu \rightarrow V(3d^34s^2)^4F+e^-$ ,  $V^-(3d^44s^2)^5D+h\nu \rightarrow V(3d^34s^2)^4P+e^-$ , and at discrete wavelengths in the region 457.9–647.1 nm using the laser photoelectron spectroscopy technique. Photoelectron yields were obtained by measuring the laboratory frame energy spectra of photodetached electrons as a function of the angle between the velocity vector of the outgoing photoelectrons and the polarization direction of the linearly polarized photon beam. A nonlinear curve-fitting routine was used to extract the value of the asymmetry parameter for a particular transition at fixed photon energies. Asymmetry parameters are also reported for photodetached  $s$  electrons in the transitions  $V^-(3d^44s^2)^5D+h\nu \rightarrow V(3d^44s)^6D+e^-$  and  $V^-(3d^44s^2)^5D+h\nu \rightarrow V(3d^44s)^4D+e^-$  at four photon energies.

DOI: 10.1103/PhysRevA.71.042708

PACS number(s): 32.80.Gc, 32.10.-f, 33.60.-q

### I. INTRODUCTION

Significant advances in laser and negative ion beam technology have stimulated numerous experimental and theoretical investigations of negative-ion photon interactions within the last three decades. In particular, photodetachment studies have played a vital role in revealing fundamental features in negative ion-photon interactions, electron-electron interactions, and in the structure of the negative ion itself [1–4]. The photodetachment process can be perceived as a two-stage phenomenon. The first stage involves the photon interacting with the negative ion. The second stage involves the outgoing electron interacting with the residual core. Since the photodetachment process results in a neutral residual core, it allows one to study weak effects (e.g., as electron correlation and relativistic interactions) that can be overwhelmed by long-range Coulomb interactions that are inherent in photoionization processes. In contrast to total cross-section measurements which provide information on the magnitudes of transition amplitudes, the differential cross section, moreover, photoelectron angular distribution measurements, provide information on their relative phases. Furthermore, photoelectron angular distribution measurements allow one to extract information regarding the initial and final states of the negative ion as well as the dynamics of the interaction itself. These distributions are generally measured using the laser photoelectron spectroscopy technique

(LPES), where relative photoelectron production is measured as a function of the angle  $\theta$  between the direction of the outgoing electron and the polarization direction of a linearly polarized laser beam.

For a single-photon, single-electron, photodetachment process, Cooper and Zare [5] have shown that angular distributions can be described by

$$\frac{d\sigma}{d\Omega} \propto 1 + \beta P_2(\cos \theta), \quad (1)$$

where  $P_2(\cos \theta)$  is the second-order Legendre polynomial and  $\beta$  describes the anisotropy of the outgoing electrons. The asymmetry parameter  $\beta$  depends on the angular momentum transferred,  $\mathbf{j}_i$ , to the photodetached electron in the photodetachment process. Equation (1) is equally valid for any unpolarized single- and multielectron targets interacting with linearly polarized photons of energy  $h\nu < 100$  eV. It has the same form for either LS or  $j$ - $j$  coupling, though the predicted value of  $\beta$  will differ if spin-orbit coupling is significant. Since the cross sections are non-negative,  $\beta$  is restricted to the range  $-1 \leq \beta \leq 2$ . If there is more than one value of angular momentum transfer, the asymmetry value is a weighted average of the form

$$\beta = \frac{\sum \sigma(j_i)\beta(j_i)}{\sum \sigma(j_i)}, \quad (2)$$

where the summations extend over all allowed values of angular momentum transfer  $\mathbf{j}_i$ . The summands  $\beta(j_i)$  and  $\sigma(j_i)$  are the partial asymmetry values and partial cross sections for that particular  $\mathbf{j}_i$ , respectively. The Cooper-Zare [5] formalism assumes a central-potential model, and the photode-

\*Present address: Physics Department, Rice University, Houston, TX 77005, USA.

†Present address: National Renewable Energy Laboratory, Golden, CO 80401, USA.

tachment process involves only the interaction of the photon with the photodetached electron (the independent-particle model), thereby neglecting the interactions of the photoelectron with the residual atomic core. This approximation restricts the allowed angular momentum transfer to be equal to the initial orbital angular momentum  $\mathbf{l}_o$  of the photodetached electron plus or minus one unit of angular momentum, i.e.,  $\mathbf{j}_t = \mathbf{l}_o \pm \mathbf{1}$ . Another limitation of the Cooper-Zare theory is that it cannot describe the energy dependence of the asymmetry parameter for systems in which configuration interaction and relativistic effects significantly affect the photodetachment process.

A more detailed formalism which overcomes these limitations and treats both stages of the photodetachment process was initially developed by Fano and Dill [6–9]. This formalism is referred to as the “angular momentum transfer theory,” and accounts for the coupling of the angular momentum of the photodetached electron to the orbital angular momentum of the residual atomic core. To illustrate this theory [9] in a system described by LS coupling, consider a negative ion (initial state) having total orbital angular momentum, total angular momentum, and parity quantum numbers  $L_o$ ,  $J_o$ , and  $\pi_o$ . Likewise, those quantum numbers for the residual atomic core following photodetachment would be  $L_c$ ,  $J_c$ , and  $\pi_c$  and

those of the outgoing photodetached electron would be  $l$ ,  $j$ ,  $\pi_e = (-1)^l$ . The photon initiates an electric dipole transition in the system, which imparts one unit of angular momentum ( $j_\gamma = 1$ ) and changes the parity of the system ( $\pi_\gamma = -1$ ). The allowed values of angular momentum transfer  $\mathbf{j}_t$  are defined by the vector equation  $\mathbf{j}_t \equiv \mathbf{j}_\gamma - \mathbf{1}$ , which can also be written as  $\mathbf{j}_t = \mathbf{L}_c - \mathbf{L}_o$ , since angular momentum is conserved  $\mathbf{J}_{\text{initial}} - \mathbf{J}_{\text{final}} = (\mathbf{J}_o + \mathbf{j}_\gamma) - (\mathbf{J}_c + \mathbf{j}) = \mathbf{0}$  and electric dipole transitions do not affect the intrinsic angular momentum states. Parity is also conserved in the photodetachment process  $\pi_{\text{initial}} = \pi_{\text{final}} = \pi_o \pi_\gamma = \pi_c \pi_e$  which reduces to the requirement  $\pi_o \pi_c = (-1)^{l+1}$ . The photodetachment process can follow either a “parity-favored”  $\pi_o \pi_c = (-1)^{l_t}$ , where  $j_t = l \pm 1$  path, or a “parity-unfavored”  $\pi_o \pi_c = (-1)^{j_t+1}$ , where  $j_t = l$  path. Fano and Dill [6–8] showed that the asymmetry parameters depend on whether the photodetachment process is parity-favored or -unfavored and can be written in terms of the fundamental complex photodetachment scattering amplitudes  $S_l(j_t)$  from which cross sections are based. These scattering amplitudes generally depend on the angular momentum transfer and photon energy. Following Ref. [9] the parity-favored quantities are

$$\beta_{fav} = \frac{(j_t + 2)|S_+(j_t)|^2 + (j_t - 1)|S_-(j_t)|^2 - 3[j_t(j_t + 1)]^{1/2}[S_+(j_t)S_-^*(j_t) + S_+^*(j_t)S_-(j_t)]}{(2j_t + 1)[|S_+(j_t)|^2 + |S_-(j_t)|^2]}, \quad (3)$$

$$\sigma_{fav} = \frac{(2j_t + 1)}{2L_o + 1} [ |S_+(j_t)|^2 + |S_-(j_t)|^2 ], \quad (4)$$

whereas the parity-unfavored photodetachment quantities are

$$\beta_{unf} = -1, \quad (5)$$

$$\sigma_{unf} = \frac{(2j_t + 1)}{2L_o + 1} |S_o(j_t)|^2. \quad (6)$$

The subscripts on the scattering amplitudes  $\pm, o$  indicate the orbital angular momentum of the outgoing photoelectron,  $l = j_t \pm 1$  or  $l = j_t$ , respectively. Thus, measurements of the asymmetry parameter provide useful insight into the angular momentum transfer (or sharing) between the outgoing photoelectron and the residual atomic core and how the angular momentum of the photon coupled with the initial negative-ion state. The energy dependence of  $\beta$  provides an indication of the importance of relativistic effects present in the atomic structure of that particular atom [9].

Since the pioneering work of Hall and Siegel [10] and Cooper and Zare [5], all experimental and theoretical studies on photoelectron angular distributions resulting from laser-negative ion interactions have focused on the photodetachment of  $s$  and  $p$  electrons. In addition, there have been relatively few experimental investigations and no theoretical

analysis regarding the spectral dependence of photoelectron angular distributions from transition-metal negative ions.

Feigerle *et al.* [11] obtained structural details of  $V^-$  with the LPES technique. Its ground-state configuration was inferred from measured photoelectron spectra, and was found to be  $(3d^4 4s^2)^5 D$  with a binding energy of  $0.526 \pm 0.012$  eV. Fine-structure splitting of the  $V^-(3d^4 4s^2)^5 D$  ground state was not resolved in this experiment. Since a fixed frequency Ar<sup>+</sup> laser (488.0 nm) was used in their measurement, four transitions from the ground-state parent ion to states of the neutral atom were observed. The observed transitions were

$$V^-(3d^4 4s^2)^5 D + h\nu \rightarrow V(3d^3 4s^2)^4 F + e^-(kp, kf), \quad (7)$$

$$V^-(3d^4 4s^2)^5 D + h\nu \rightarrow V(3d^4 4s)^6 D + e^-(kp), \quad (8)$$

$$V^-(3d^4 4s^2)^5 D + h\nu \rightarrow V(3d^4 4s)^4 D + e^-(kp), \quad (9)$$

$$V^-(3d^4 4s^2)^5 D + h\nu \rightarrow V(3d^3 4s^2)^4 P + e^-(kp, kf), \quad (10)$$

and are illustrated in the energy-level diagram in Fig. 1. In this paper, we augment the previous study by reporting photoelectron angular measurements (asymmetry parameters) resulting from a single-photon, single-electron photodetachment of both  $s$  and  $d$  electrons from  $V^-$  for the four transitions listed above. The measurements have been carried

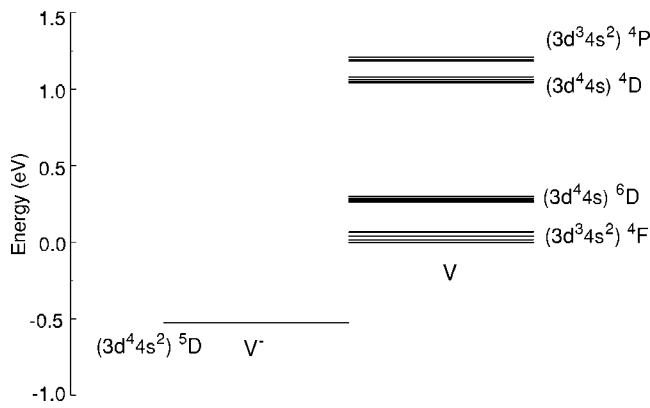


FIG. 1. Energy level diagram of  $V^-$  and  $V$ . The energy levels shown in the figure are inferred from the measurements from Feigerle *et al.* [11].

out at discrete photon wavelengths ranging from 457.1 nm to 647.1 nm with a crossed ion-laser beams apparatus that utilizes the LPES technique to examine the photon energy dependence of the asymmetry parameters, which are sensitive to the angular momentum coupling between the negative ion and atomic cores, the photoelectron, and the photon.

## II. EXPERIMENT

Thorough descriptions of the experimental apparatus along with benchmark tests have been presented elsewhere [12,13]. However, a brief overview of the apparatus is presented below for continuity. Figure 2 presents a schematic diagram of the LPES apparatus. The  $V^-$  ion beam is produced in a cesium-sputter, negative ion source [14]. The source operates by thermally ionizing cesium atoms and accelerating the resulting  $Cs^+$  ions towards a negatively biased vanadium-gallium pellet. Negative ions resulting from the pellet- $Cs^+$  collision were accelerated to a potential of 10 kV and focused into a beam. The  $V^-$  ions were momentum selected by passing the extracted beam through a double focusing,  $90^\circ$  bending magnet, thereby resulting in an isotopically pure  $^{51}V^-$  ion beam. The mass resolution of the magnet was

approximately 0.5%. After traversing the exit aperture of the magnet, the mass selected  $^{51}V^-$  ions were focused and steered into the interaction chamber whose base pressure was  $1 \times 10^{-7}$  Pa. Typical  $^{51}V^-$  beam intensities inside the interaction chamber ranged from 10 to 30 nA. A  $^{50}V^-$  beam was also observed (10–50 pA). The ratio of beam intensities  $^{51}V^-/^{50}V^-$  was of the same order as the relative abundance of the two isotopes. However, the  $^{50}V^-$  beam was not sufficiently intense to allow photoelectron angular distribution measurements.

Inside the interaction chamber, the  $^{51}V^-$  beam intersected a linearly, polarized, continuous (cw) photon beam from either a 25 W  $Ar^+$  laser or a 1 W  $Kr^+$  laser at  $90^\circ$ . The 25 W  $Ar^+$  and the 1 W  $Kr^+$  laser (with the aid of an external prism for wavelength selection) operated in a polarized single-line mode to produce photon beams ranging from 0.25 W to 13 W. The photon beam from either laser passed through a Glan-Laser polarizing prism and a double Fresnel rhomb ( $\lambda/2$  retarder) before entering the interaction chamber. Since the extinction ratio of the polarizer was greater than  $5 \times 10^{-5}$ , high polarization purity was guaranteed. To vary the angle between the outgoing electrons and the polarization direction of the photon beam, the photoelectron collection direction was fixed while the polarization direction of the photon beam was rotated with the  $\lambda/2$  retarder. The positioning of the two beams was aided by sets of apertures near the interaction region. The overlap between the ion and laser beams was carefully maximized by positioning the photon beam while minimizing laser beam translations due to rotations of the  $\lambda/2$  retarder.

Photoelectrons produced during the ion-photon interaction were energy-analyzed by a  $160^\circ$  spherical-sector electron spectrometer that was placed 45 degrees below the horizontal plane formed by the crossed ion and laser beams. The electron energy analyzer was operated at constant pass energies of 20 eV or 40 eV, depending on the photoelectron yield for a particular transition. A comparison of the measured angular distributions for a particular transition indicated excellent agreement in the data for the different pass energies of 20 and 40 eV. The energy resolution of the spectrometer was approximately 0.4%, and was determined from the full width at half-maximum of the measured photoelectron spec-

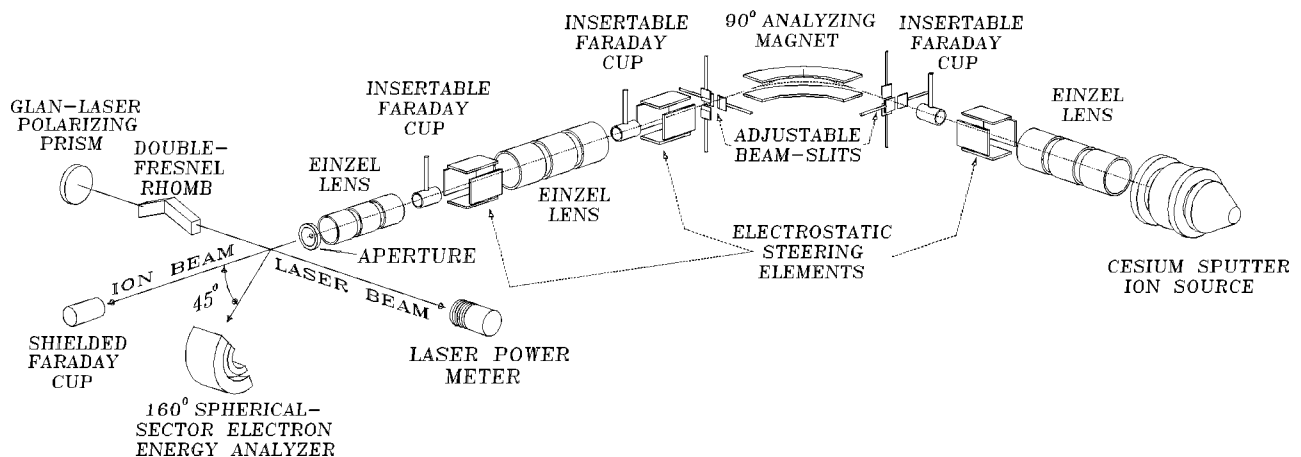


FIG. 2. Schematic diagram of the experimental apparatus.

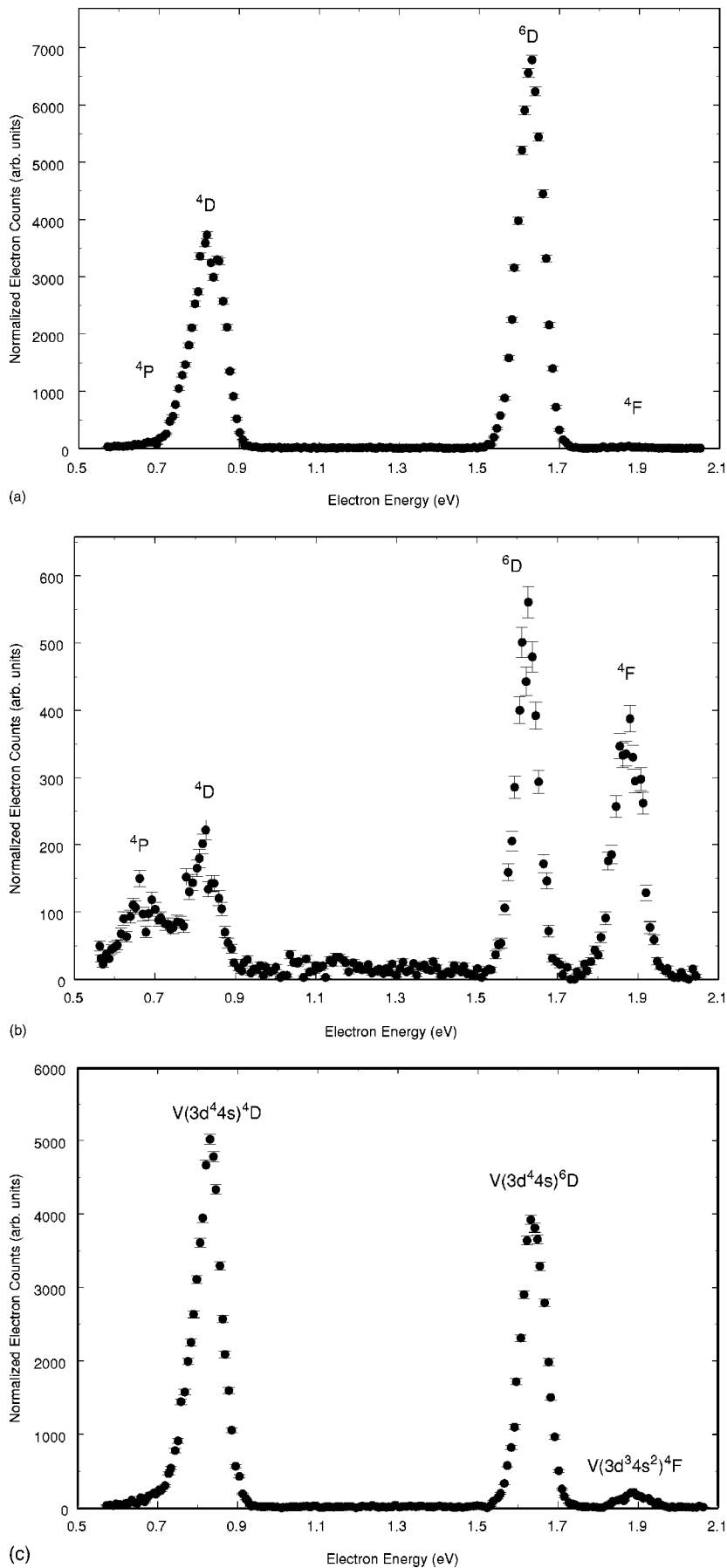


FIG. 3. Photoelectron energy spectra for  $h\nu + V^- \rightarrow V + e^-$ . The observed transitions agree with those of Feigerle *et al.* [11]. The photoelectron peaks are labeled by their final-state term designations for vanadium. The energy and angle-resolved spectra were measured with the 514.5 nm line of a cw Ar<sup>+</sup> laser. (a) Observed photoelectrons when the polarization direction of the photon beam was  $-3.4^\circ$  relative to the velocity vector of the collected photoelectrons. Note the dominance of the  $V^-(3d^4 4s^2)^5D + h\nu \rightarrow V(3d^4 4s)^6D + e^-$  and  $V^-(3d^4 4s^2)^5D + h\nu \rightarrow V(3d^4 4s)^4D + e^-$  transitions at this angle. (b) Observed photoelectrons when the polarization direction of the photon beam was  $86.6^\circ$  to the velocity vector of the collected photoelectrons. Note the appearance of the  $V^-(3d^4 4s^2)^5D + h\nu \rightarrow V(3d^3 4s^2)^4F + e^-$  and  $V^-(3d^4 4s^2)^5D + h\nu \rightarrow V(3d^3 4s^2)^4P + e^-$  transitions. (c) Observed photoelectron spectrum when the polarization direction of the photon beam was  $56.6^\circ$  relative to the velocity vector of the collected photoelectrons.

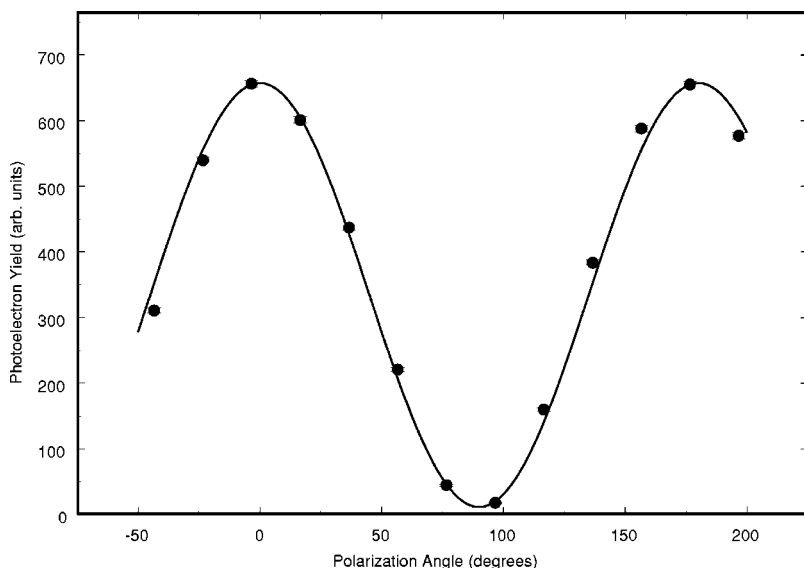


FIG. 4. A typical plot of the photoelectron yields for the transition  $V^-(3d^4 4s^2)^5 D + h\nu \rightarrow V(3d^4 4s)^6 D + e^-$  versus the angle between the polarization direction of the photon beam and the photoelectron collection direction. The extracted value of  $\beta$  for this particular angular distribution measurement at 514.5 nm is  $1.90 \pm 0.04$ . The error bar in  $\beta$  reflects the statistical uncertainty of the nonlinear curve fit described in the text. A plot for the  $V^-(3d^4 4s^2)^5 D + h\nu \rightarrow V(3d^4 4s)^4 D + e^-$  is not shown since it is similar to the one shown here.

tra. The acceptance angle was limited to angles less than  $1^\circ$  by a pair of entrance apertures and the 31.8 mm distance from the first entrance aperture and the center of the interaction region. All nearby materials were coated with Aerodag G, thereby minimizing contact potentials in the vicinity of the electron spectrometer and the interaction region. Electrons with the proper energy for transmission through the spectrometer were collected with a channeltron electron multiplier. All high voltage contacts of the photoelectron detection system were carefully shielded from the interaction region. In addition, the electron spectrometer and the interaction region were shielded from stray magnetic fields, which reduced the magnitude of the magnetic field in the interaction region to less than 5 mG.

A preamplifier and amplifier successively boosted signals produced by the channeltron before entering a constant fraction discriminator, which reduced background noise. A computer-controlled counter collected output pulses from the discriminator. Additional computer-controlled counters monitored output pulses from two voltage-to-frequency converters that were used to convert analog signals from a laser power meter and an electrometer. The additional counters were used to monitor the intensity of the ion and photon beams to normalize the photoelectron signal. Data from the counters were processed and stored with a data acquisition and control program. The data accumulation time for each data point varied from 2 to 10 s.

Photoelectron spectra were collected and stored as a function of the voltage applied to the spectrometer for a particular value of  $\theta$ . The angle  $\theta$  was varied in  $10^\circ$  increments by rotating the double Fresnel rhomb in  $5^\circ$  increments. Typical energy- and angle-resolved spectra measured at a wavelength of 514.5 nm are shown in Fig. 3. The relative intensities of the observed transitions were found to be in excellent agreement with those observed by Feigerle *et al.* [11]. In Fig. 3(a), the polarization direction of the photon beam and the electron collection direction are parallel. At this polarizer setting, the photoelectron yield for the  $V^-(3d^4 4s^2)^5 D + h\nu \rightarrow V(3d^4 4s)^6 D + e^-$  process is near a maximum, while the yield for the  $V^-(3d^4 4s^2)^5 D + h\nu \rightarrow V(3d^3 4s^2)^4 F + e^-$  transi-

tion is near a minimum. When the polarization direction of the photon beam is nearly perpendicular to the photoelectron collection direction [refer to Fig. 3(b)], the  $V^-(3d^4 4s^2)^5 D + h\nu \rightarrow V(3d^4 4s)^6 D + e^-$  is near a minimum, while the yield for the  $V^-(3d^4 4s^2)^5 D + h\nu \rightarrow V(3d^3 4s^2)^4 F + e^-$  is near a maximum.

To determine the photoelectron yield for each peak, the spectra were fitted to a linear combination of a Gaussian and a linear background function, using a nonlinear least-squares routine that weighted each data point by its statistical uncertainty. Once the fitting parameters were extracted from the fit, each Gaussian was integrated to obtain the photoelectron yield and its uncertainty. The yields for each transition were plotted as a function of the dial setting on the polarization rotator, and fitted to the equation

$$I(\theta) = a\{1 + \beta P_2[\cos(\alpha - c)]\}, \quad (11)$$

where  $a$ ,  $\beta$ , and  $c$  are fitting parameters, and  $\alpha$  is the dial setting of the polarization rotator. The dial setting of the polarization rotator (double-Fresnel rhomb) does not necessarily correspond with  $\theta$ , the angle between the photoelectron collection direction and the polarization direction of the photon beam. As a result, the angular origin for  $\theta$  had to be determined. The procedure for this calibration process is straightforward. First, a polarization analyzer with its transmission axis parallel to the electron collection direction was inserted into the laser beam beyond the double-Fresnel rhomb. Then electrons were collected from a photodetachment process whose asymmetry parameter is known to be near  $-1$ . The dial setting of the polarization rotator was varied until a minimum photoelectron yield was observed. The angular origin was easily ascertained, once the dial setting of the double-Fresnel rhomb was calibrated to  $(\theta = 90^\circ)$ . Plots of typical photoelectron yields as a function of  $\theta$  are shown in Figs. 4 and 5.

### III. RESULTS AND DISCUSSION

The measured asymmetry parameters for all transitions and photon energies are listed in Table I. Each cell in the

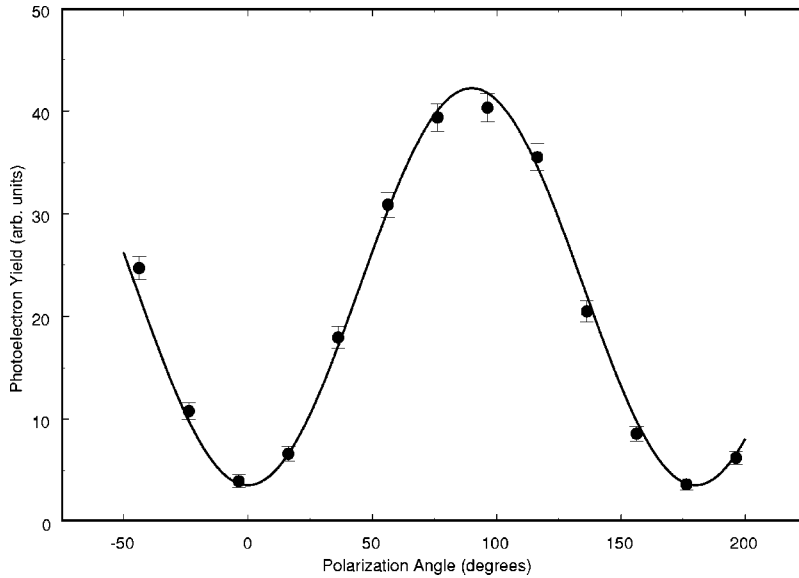


FIG. 5. A typical plot of the photoelectron yields for the transition  $V^-(3d^44s^2)^5D+h\nu \rightarrow V(3d^34s^2)^4F+e^-$  versus the angle between the polarization direction of the photon beam and the photoelectron collection direction. The extracted value of  $\beta$  for this particular angular distribution measurement at 514.5 nm is  $-0.88 \pm 0.01$ . The error bar in  $\beta$  reflects the statistical uncertainty of the nonlinear curve fit described in the text.

table displays the weighted average of several measured asymmetry parameters with error bars based on the statistical uncertainties of the nonlinear curve fits. The mean values of the extracted asymmetry parameters were used to estimate systematic errors. The largest systematic error was due to the variation in spatial overlap of the laser and ion beams. All error bars in Table I are reported to one standard deviation from the mean. Since the entrance aperture of the electron spectrometer was sufficiently small, solid angle corrections to the measured asymmetry parameters were not required.

To gain some insight into the nature of the interaction between the  $V^-$  and the photon beam, it is important to examine the experimental results within the framework of the Cooper-Zare [5] theory and the angular momentum transfer formalism. Within the Cooper-Zare [5] theory, the photodetachment process produces an outgoing  $p$  wave when the  $s$  electron is photodetached from the parent ion, and  $p$ - or  $f$ -wave photoelectrons when the  $d$  electron is photodetached from  $V^-$ . In the case when the  $s$  electron is photodetached from the negative ion, the independent-particle approximation predicts an energy-independent asymmetry parameter,  $\beta=2$ . A comparison between this theoretical prediction and the measured  $\beta$  parameters (see Table I) for the processes  $V^-(3d^44s^2)^5D+h\nu \rightarrow V(3d^44s)^6D+e^-$  and  $V^-(3d^44s^2)^5D+h\nu \rightarrow V(3d^44s)^4D+e^-$  indicates agreement over all observed photon energies. According to the Cooper-Zare

model, the relative contribution of  $p$  and  $f$  waves resulting from the ejection of the  $d$  electron of  $V^-$  depends on the energy of the incoming photon beam and the structure of the negative ion. If  $p$  waves dominate, the asymmetry parameter approaches a value of 0.2, but if the  $f$  wave dominates it approaches a value of 0.8. The minimal and maximal value of  $-1$  and  $2$ , respectively, can only occur when the outgoing  $p$  and  $f$  waves interfere. To the authors' knowledge, a calculation that predicts the asymmetry parameter or the relative contribution of the outgoing  $p$  or  $f$  waves for this process has not been carried out. One should expect the  $p$  wave to dominate near threshold, since the centrifugal barrier better suppresses the high angular momentum of the  $f$  wave [15]. However, all  $\beta$  parameters reported in Table I result from processes far from threshold, which leads one to expect both  $p$  and  $f$  partial waves to interfere. Since the results in Table I are near  $-1$  for the  $d$  electron process  $V^-(3d^44s^2)^5D+h\nu \rightarrow V(3d^44s^2)^4F+e^-$ , one can infer that both partial waves contribute significantly in the photodetachment process. In the case of the  $V^-(3d^44s^2)^5D+h\nu \rightarrow V(3d^34s^2)^4P+e^-$  process, one needs additional theoretical details to deduce the dominant interaction.

To express the asymmetry parameter within the angular momentum transfer theory, one must first list all allowed angular momentum transfer  $j_i$ . Table II lists the allowed values of  $j_i=|\mathbf{L}_c-\mathbf{L}_0|$  for each transition along with their corre-

TABLE I. Photoelectron asymmetry parameters for the process  $(h\nu+V^- \rightarrow V+e^-)$ . The transitions are labeled by the final states in V.

Wavelength (nm)	$V(3d^34s^2)^4F$	$V(3d^34s^2)^4P$	$V(3d^44s)^6D$	$V(3d^44s)^4D$
457.9			$1.96 \pm 0.01$	$1.99^{+0.01}_{-0.02}$
476.0	$-0.99^{+0.05}_{-0.01}$		$1.98 \pm 0.02$	$1.98 \pm 0.02$
488.0	$-0.93 \pm 0.03$	$-0.4 \pm 0.1$	$1.92 \pm 0.03$	$1.95 \pm 0.01$
496.0	$-0.85 \pm 0.04$		$2.00^{+0.00}_{-0.08}$	$2.00^{+0.00}_{-0.01}$
514.5	$-0.93 \pm 0.02$	$-0.3 \pm 0.1$	$1.91 \pm 0.03$	$1.99^{+0.01}_{-0.02}$
647.1				$2.00^{+0.00}_{-0.04}$

TABLE II. Allowed values of  $j_i$  and the parity-favored and -unfavored values for  $j_i$  for the observed transitions. Also listed are the possible outgoing waves predicted by the interchannel-electron correlation (in parentheses). Note the initial ion and all final states are even, resulting in parity-favored and parity-unfavored processes determined by even and odd values of  $j_i$ , respectively.

Final atomic state	Angular momentum transfer $j_i= L_c-L_o $	Parity-favored $j_i$	Parity-unfavored $j_i$	Outgoing $e^-$ $l_o\pm 1$
$V(3d^34s^2)^4F$	1,2,3,4,(5)	2,4	1,3,(5)	$p$ and $f(h)$
$V(3d^34s^2)^4P$	1,2,3	2	1,3	$p$ and $f$
$V(3d^44s)^6D$	0,1,2,(3,4)	0,2,(4)	1,(3)	$p$ and $(f)$
$V(3d^44s)^4D$	0,1,2,(3,4)	0,2,(4)	1,(3)	$p$ and $(f)$

sponding parity favored and unfavored values. The angular momentum transfer theory allows more values of  $j_i$  due to the angular momentum coupling of the photon with the negative ion and the residual atomic core than the independent particle model for the transitions in the current study. This results in the allowance of more partial waves interfering for the outgoing photoelectron. However, as stated in Ref. [9], the effects from the higher odd  $-1$  values may be small. Any deviation of the asymmetry parameter predictions from the measured values or those displaying an energy dependence will indicate the need for the more sophisticated angular momentum theory and be an indication of the electron correlation effects.

A comparison of the  $s$ -electron photodetachment results to the expression for  $\beta(^4D)$  and  $\beta(^6D)$  indicates that the  $j_i=l_o$  angular momentum transfer dominates these photodetachment processes at the measured photoenergies. The asymmetry parameters also do not display a pronounced energy dependence within the range of photon wavelengths of this experiment. This suggests that the final-state interaction between the residual atomic vanadium core and the outgoing electron is weak. Furthermore, the liberated electron can be described by a  $p$  wave in agreement with the Cooper-Zare theory [5]. In the case of  $d$ -electron photodetachment, we do not have sufficient evidence to rule out parity-favored or -unfavored channels in the observed values of  $\beta$  near  $-1$ , since parity-favored channels can interfere to yield asymmetry parameters near negative 1. A complete theoretical calculation is needed to discern which channels dominate.

#### IV. CONCLUSIONS

Asymmetry parameters have been measured for the single-photon, single-electron photodetachment of  $s$  and  $d$  electrons from  $V^-$  at discrete wavelengths in the region 457.9–647 nm. The results were discussed within the Cooper-Zare [5] theory and the angular momentum transfer formalism of Fano and Dill [6–9]. The analysis of the processes involving the photodetachment of an  $s$  electron from  $V^-$  over the discrete photon energies suggests that final-state interactions between the outgoing electron and the residual  $V$  atom are weak, indicating that the Cooper-Zare [5] theory provides a satisfactory description of the observed process. In the processes involving the photodetachment of a  $d$  electron for  $V^-$ , the measured values of the asymmetry parameter near  $-1$  for the  $V^-(3d^44s^2)^5D+h\nu\rightarrow V(3d^34s^2)^4F+e^-$  transition imply that both  $p$  and  $f$  partial waves may contribute significantly to the observed processes. A comparison between the Cooper-Zare [5] and Fano-Dill [6–9] description for  $d$  electron photodetachment processes requires a complete theoretical calculation of the observed process.

#### ACKNOWLEDGMENTS

This work was supported by the National Science Foundation under Cooperative Agreement OSR-935227. T.J.K. acknowledges support from a grant from the Division of Chemical Sciences, Office of Basic Energy Sciences, Office of Energy Research, U.S. Department of Energy.

- 
- [1] C. Blondel, Phys. Scr., T **T58**, 31 (1995).  
 [2] T. Andersen, Phys. Scr., T **T34**, 23 (1991).  
 [3] T. Andersen, H. K. Haugen, and H. Hotop, J. Phys. Chem. Ref. Data **28**, 1511 (1999).  
 [4] D. R. Bates, Adv. At., Mol., Opt. Phys. **27**, 23 (1991).  
 [5] J. Cooper and R. N. Zare, J. Chem. Phys. **48**, 942 (1968).  
 [6] U. Fano and Dan Dill, Phys. Rev. A **6**, 185 (1972).  
 [7] D. Dill and U. Fano, Phys. Rev. Lett. **29**, 1203 (1972).  
 [8] D. Dill, A. F. Starace, and S. T. Manson, Phys. Rev. A **11**, 1596 (1975).  
 [9] S. T. Manson and A. F. Starace, Rev. Mod. Phys. **54**, 389 (1982).  
 [10] J. L. Hall and M. W. Siegel, J. Chem. Phys. **48**, 943 (1968).  
 [11] C. S. Feigerle, R. R. Corderman, S. V. Bobashev, and W. C. Lineberger, J. Chem. Phys. **74**, 1580 (1981).  
 [12] A. M. Covington, D. Calabrese, W. W. Williams, J. S. Thompson, and T. J. Kvale, Phys. Rev. A **56**, 4746 (1997).  
 [13] D. Calabrese, A. M. Covington, D. L. Carpenter, J. S. Thompson, T. J. Kvale, and R. L. Collier, J. Phys. B **30**, 4791 (1997).  
 [14] Kingston Scientific Inc., Kingston, TN 37763.  
 [15] E. P. Wigner, Phys. Rev. **73**, 1002 (1948).